J Mater Sci (2007) 42:2267–2275
DOI 10.1007/s10853-006-0827-8

4TH BRAZILIAN MRS MEETING

# Numerical and experimental analysis of microstructure formation during stainless steels solidification

**M. L. N. Melo · Carlos Lima Penhalber · Nilton Alves Pereira · Carmo Lima Pelliciari Jr. · Carlos A. Santos**

Received: 4 November 2005 / Accepted: 21 August 2006 / Published online: 6 February 2007


**Abstract** The aim of this work is to examine microstructure formation during the solidification of unidirectional solidified AISI 304 stainless steel. Numerical and experimental results indicate that this numerical model allows a precise analysis of the AISI 304 stainless steel microstructure formation. This model determines temperature profiles, position of liquid and solid isotherms, thermal parameters (thermal gradients, tip rate movement, rate cooling), and finally, the secondary inter dendritic spacing. This model was tested by comparing the experimental values results, and thus a reasonable correlation was found.

## Introduction

Stainless steel is used for a variety of components by virtue of its excellent corrosion resistance, heat resistance and good appearance [1]. Stainless steels are iron based alloys that contain at least 11% chromium, the quantity needed to guarantee high resistance to corrosion at room temperature. Other elements are added to improve special characteristics as for example: molybdenum, vanadium, copper, titanium, aluminum, silicon, niobium, nitrogen, sulfur and selenium, carbon and particularly nickel with a content of up 8% [2]. Stainless steels are classified into four types, considering their micro-structural characteristics: ferritic, austenitic, martensitic and duplex (austenite and ferrite) [2–4].

It is generally found that the mechanical properties (notably strength, ductility, corrosion and oxidation resistance and fatigue life) on a metallic material increase as the grain size decreases. The well-known Hall-Petch equation shows that the yield strength is proportional to the reciprocal of the square root of the grain diameter [5]. As for fatigue cracks, originating material defects, flaws and inclusions, cracks can gradually grow in the low stress cycles conditions even under yield stress. Most fatigue life parts are usually spent during a generating period before cracks are clearly significant and while micro cracks are stably growing in 1–3 grains [6]. It is reasonable to assume that the coarse grain size might have shortened the crack initiation stage. Furthermore, in alloys deforming by planar slip, an improved crack propagation resistance has been noticed with decreasing grain size and has been ascribed to the fact that the grain boundaries serve as natural barriers to transgranular crack propagation, causing the crack front to be held back and needing a crack reinitiating event to occur in each new grain [7]. Therefore, in order to control the properties of materials, it is important to understand the

M. L. N. Melo (✉) · C. L. Penhalber · N. A. Pereira
Programa de Pós-graduação em Engenharia e Ciência dos Materiais, Universidade São Francisco (USF), Rua Alexandre de Rodrigues Barbosa, 45, 13251-900 Itatiba, SP, Brazil
e-mail: mirian.melo@saofrancisco.edu.br

C. L. Pelliciari Jr.
Departamento de Engenharia de Materiais, Faculdade de Engenharia Mecânica, Universidade Estadual de Campinas (UNICAMP), Campinas, SP, Brazil

C. A. Santos
Departamento de Engenharia Mecânica e Mecatrônica, Faculdade de Engenharia, Pontifícia Universidade Católica do Rio Grande do Sul (PUCRS), Porto Alegre, RS, Brazil

solidification parameters that affect the microstructure and growth of grains during solidification.

During the solidification of alloys, the microstructures observed are diverse, but in general, they can be classified into two basic groups: cell/dendrites and eutectic morphologies. Dendrite growth is the common mechanism of crystallization from metallic melts, and the morphology that is formed consists of an array of dendrites with a side branch configuration. The solute, which is redistributed due to the solubility difference between the solid and liquid phases provokes an important consequence on such structure, i.e., the occurrence of micro-segregation between the dendrite branches [8]. The dendritic array characterized by the primary and secondary spacing and the segregated products, greatly affects solidified alloys [8]. On the other hand, dendrite spacing is controlled by the growth rate (V) and the temperature gradient (G) [9], for a given composition, i.e., by relationships between solidification conditions.

Solidification phenomena modeling during the casting process has had widespread application in the industry as a tool to understand and improve product quality. Solidification modeling is used to analyze and develop the casting processes of cast products. It may also provide new foundations for various phenomena occurring during the casting process. During the last years, computer based numerical modeling has been used to study the solidification processes and to predict the microstructure of castings, especially with aluminum alloys [10–16]. The aim of this work is to examine the microstructure formation during the solidification of unidirectional solidified AISI 304 stainless steel specially the arm secondary spacings on a numerical simulation and comparing with the experimental values results.

## Mathematical modeling

Considering that solidification of alloys is primarily governed by heat diffusion, the basic continuity equation at macroscopic scale is the equation of energy conservation, given by [17]:

$$\rho \cdot c_p \cdot \frac{\partial T}{\partial t} = \nabla \cdot (k \cdot \nabla T) + Q \tag{1}$$

Where $\rho$ is the solid metal density, $c_p$ is the solid metal specific heat, $k$ is the solid metal thermal conductivity, $Q$ is the heat liberated during solidification, $T$ is the temperature, $t$ is the time.

The heat liberated during solidification is taken into account applying the enthalpy model. The solid fraction as the temperature function is determined using the Scheil equation [18] and the variation curve of enthalpy versus temperature can be calculated:

$$Q = \rho \cdot L_m \cdot \frac{\partial f_s}{\partial t} \tag{2}$$

Where $L_m$ is the latent heat of solidification, $f_s$ is the solid fraction.

From Eqs. 1 and 2:

$$\rho \cdot c_p \cdot \frac{\partial T}{\partial t} - \rho \cdot L_m \cdot \frac{\partial f_s}{\partial T} \cdot \frac{\partial T}{\partial t} = \nabla \cdot (k \cdot \nabla T) \tag{3}$$

As enthalpy ($H$) is given by:

$$H = \int_0^T \rho \cdot c_p \cdot \mathrm{d}T + \rho \cdot L_m \cdot (1 - f_s) \tag{4}$$

and

$$\frac{\partial H}{\partial T} = \rho \cdot c_p - \rho \cdot L_m \cdot \frac{\partial f_s}{\partial T} \tag{5}$$

From Eqs. 3 and 5:

$$\frac{\partial H}{\partial t} = \nabla \cdot (k \cdot \nabla T) \tag{6}$$

For unidirectional heat flow, Eq. 6 takes the form of:

$$\frac{\partial H}{\partial t} = k \cdot \frac{\partial^2 T}{\partial x^2} \tag{7}$$

Considering a chilled (cooled) mold, a balance of energy in the metal/mold interface results in:

$$-k \cdot \frac{\partial T}{\partial x} - hi \cdot (T_i - T_0) = 0 \tag{8}$$

Where $hi$ is the heat transfer coefficient at the metal/mold interface, $T_i$ is the temperature at metal/mold interface, $T_0$ is the temperature of the coolant.

Following a suitable discretization of the metal/mold system, the differential equations are solved using the finite differences method [19]. Temperatures are determined from the enthalpy values, using the variation curve of enthalpy versus temperature, and the thermal parameters: the thermal gradients in the front side of the dendrite tip ($G_{\mathrm{liq}}$), the advance velocities of

dendrite tip ($V_{liq}$), the local solidification time ($t_{local}$), and finally the cooling rate ($R$).

To determine the thermal gradient front side *liquidus* and the advance velocity of this front side, the following equations were applied [20–22]:

$$G_{exp} = \frac{T_{liq}^{i+1} - T_{liq}^{i}}{\Delta x} \quad (9)$$

Where $T_{liq}^{i}$ is the *liquidus* temperature in a position $i$, °C, $T_{liq}^{i+1}$ is the subsequent thermopair temperature $i + 1$ at the same instant in °C, $\Delta x$ is the distance between two adjacent thermopairs in m.

Admitting that the temperature in the dendrite tip would be equal to the *liquidus* temperature, the displacement velocity in the front side *liquidus*, can be determined with the equation:

$$V_{exp} = \frac{\Delta x}{t_{liq}^{i+1} - t_{liq}^{i}} \quad (10)$$

Where $t_{liq}^{i+1}$ is the elapsed time until the passage of the isotherm *liquidus* in a position $i$, in s, $t_{liq}^{i}$ is the elapsed time until the isotherm *liquidus* passage in the next thermopair, in s.

Solidification of alloys is characterized by the existence of a mushy zone in which the solid phase and the liquid phase coexist [10]. One important factor is the local solidification time which is known to have a strong influence on the secondary dendrite arm spacing, intermetallic content, and the porosity size and distribution [23]. It is the interval of time measured from the passage of the dendrite tip and dendrite root at each position. During this time, the secondary arms can thicken which is known as coarsening. Coarsening of the dendrite secondary arms occurs through the refusion mechanism of the thin secondary arms and the thicker arms thickening [23, 24]. The local solidification time ($t_{local}$) is defined as the time between the passage of the *liquidus* isotherm and *solidus* isotherm over a determined position, that is, the interval of time between the passage of the tip and the root of the dendrite. In the case of directional solidification [22], it gives us:

$$t_{local} = \frac{\Delta T}{R} = \frac{T_{liq} - T_{sol}}{G.V} \quad (11)$$

Where $R$ is *the* cooling rate in °C/s, $G$ is the interface temperature gradient in °C/m, $V$ is the advance velocity of the *liquidus* isotherm or of the dendrite tip in m/s, $T_{liq}$ is the *liquidus* temperature in °C, $T_{sol}$ is the *solidus* temperature in °C.

The determination of the cooling experimental rate can be done through the equation [20–22, 25]:

$$R_{exp} = \frac{\Delta T}{\Delta t_{exp}} = \frac{T_{liq} - T_{eut}}{\Delta t_{local}^{exp}} \left(^{\circ}C/_{s}\right) \quad (12)$$

Where $R_{exp}$ is the experimental cooling rate in °C/s, $\Delta T$ is the temperature variation in the mushy zone in °C, $\Delta t_{local}^{exp}$ is the time interval between the temperature *liquidus* passage ($T_{liq}$) and the eutectic temperature ($T_{eut}$) in a determinate position in s.

Consequently, to control the properties of cast alloys, it is necessary to understand the mechanism and the characterization of dendrite spacings during the solidification of alloys. For the microstructure estimate of non-ferrous there are many models of different alloys: the empirical models, specific for determinated alloys [24, 26], based exclusively on experimental results, and the theoretical ones [8, 27–29], based on thermal parameters and on geometric relations. However for ferrous alloys, in special stainless steel, few models are found in literature [9, 30]. Taha and colaborators [9] have determinated the interdentritic spacings of 30, 120, 510 mm/h and the temperature gradients varying from 13 to 187 K/cm through the directional solidification use in steel alloys with various compositions. They also applied the equation proposed by Kurz and Fisher [8], which correlates the interdentritic spacings with thermal parameters, according to equation:

$$\lambda_2 = KV^m G^n \quad (13)$$

Where $\lambda_2$ is the interdendritic spacing in cm, $V$ is the growth velocity in cm/s and $G$ is the thermal gradient in K/s, and they have determinated the values of the constants $K$, $m$ and $n$ for some compositions of interest, according to Table 1:

Tara and collaborators [9] have also used the equation proposed by Flemings [23], where the secondary spacings are related to the local solidification time, i.e., the time interval spent between the passage of the lines *liquidus* and *solidus* [8], according to the equation:

**Table 1** Equation parameters results proposed by Kurz and Fisher [8] for the secondary spacing determination [9]

| Steel composition (% weight) | Secondary spacing (cm) | | |
|---|---|---|---|
| | *K* | *m* | *n* |
| Curve 01<br>0.63 C–10.0 Mn–0.009 Si–14.9 Ni 0.095 Al–0.009 P–0.00 S | 0.0036 | –0.41 | –0.37 |
| Curve 02<br>0.63 C–1.1 Si–28.3 Cr | 0.0032 | –0.41 | –0.37 |

**Table 2** Equation parameters results proposed by Flemings [23] for the secondary spacings determination [9]

| Steel composition (% weight) | Secondary spacing (cm) | |
|---|---|---|
| | *a* | *b* |
| Curve 03<br>0.63 C–10.0 Mn–0.009 Si–14.9 Ni 0.095 Al–0.009 P–0.00 S | 0.00058 | 0.44 |
| Curve 04<br>0.63 C–1.1 Si–28.3 Cr | 0.00052 | 0.39 |

$$\lambda_2 = a.t_{\text{local}}^{b} \tag{14}$$

Where $a$ and $b$ are constant for each alloy, and $t_{\text{local}}$ is the local time of solidification (s). The results for the compositions of interest are in Table 2:

## Experiment

Figure 1 shows the experimental device used to directionally solidify the stainless steel AISI 304, with the unidirectional macrostructure obtained. The stainless steel alloy melted and poured at 1903 K in a cylindrical mold, 40 mm diameter by 250 mm length, made from insulating ceramic, in the device kept at 1773 K and water cooled from the bottom.

Temperature profiles in the casting and the mold during solidification were measured with Pt–Rh 10 pct thermocouples protected with a diameter of 0.35 mm at different positions (Fig. 1) using a data acquisition system. Small samples were cut, polished and attached in order to measure the variation in interdendritic spacings with the distance from the cooled cooper chill, using optical microscopy and the medium values of the secondary dendritic spacing, maximum and minimum for each position were presented.

## Results and discussion

A mathematical model was used to simulate solidification, and the equations are solved using an explicit finite difference method, the enthalpy method. This model considers that solidification is governed principally by thermal conduction and permits obtaining thermal profiles, solid fractions and the location of the *solidus* and *liquidus* isotherms. Besides this, it determines the principal solidification process parameters, which are thermal gradients, isotherm dislocation speed, local time of solidification and cooling rates. After determining the thermal parameters it still allows determination of the structural parameters (interdendritic spacing), by introducing the adequate equations. This model was initially used for aluminum alloy with good agreement on experimental results [14, 16, 19]; recently it was modified for stainless steels. Simulations

**Table 3** Composition of stainless steel—AISI 304

| Cr | Ni | Mn | Si | S | C | P | Co | Mo |
|---|---|---|---|---|---|---|---|---|
| 18.3 | 8.51 | 1.94 | 0.37 | 0.032 | 0.032 | 0.030 | 0.20 | 0.38 |
| W | Cu | Ti | Nb | Al | B | N2 | V | – |
| 0.57 | 0.030 | 0.005 | 0.05 | 0.005 | 0.0012 | 0.082 | 0.078 | – |

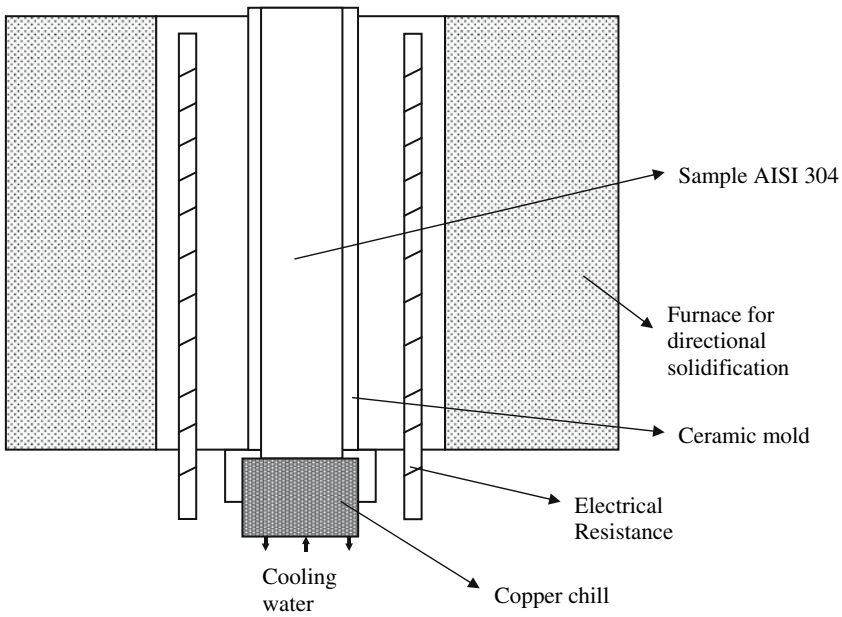


**Fig. 1** Schematic illustration of the experimental apparatus used to directionally solidify

**Table 4** Constants and thermophysical properties of AISI 304 stainless steel [31]

| Property | Value |
|---|---|
| Liquid temperature | 1454°C |
| Solid temperature | 1399°C |
| Latent heat in melting ($L$) | 290,000 kJ/kg |
| Density ($\rho$) | 8000 kg/m$^3$ |
| Thermal conductivity | Function 01 |
| Specific heat | Function 02 |
| Coefficient of solute repartition ($rk$) | 0.84 |
| and | |
| Function 01—Thermal conductivity (W/mK) | |
| $K = 10.717 + 0.014955\ T$ | $T =<780$ |
| $K = 12.076 + 0.013213\ T$ | $780 =<T =<1672$ |
| $K = 217.12 - 0.1094\ T$ | $1672 =<T =<1727$ |
| $K = 8.278 + 0.0115\ T$ | $1727 =<T$ |
| and | |
| Function 02—Specific heat (kJ/kgK) | |
| $cp = 0.43895 + 1.98 \times 10^{-4}\ T$ | $T =<353$ |
| $cp = 0.13793–5.9 \times 10^{-4}\ T$ | $773 =<T =<873$ |
| $cp = 0.87125–2.5 \times 10^{-4}\ T$ | $873 =<T =<973$ |
| $cp = 0.55520 + 7.75 \times 10^{-5}\ T$ | $973 =<T$ |

were performed with 250 mesh and interactions of 0.001 s, for a 250 mm long and 40 mm diameter part.

The present study was accomplished to examine the unidirectional solidification of the AISI 304 stainless steel during solidification against a chilled mold. Although the method is applied to the AISI 304 stainless steel, it is generally valid and can be easily extended to other systems. The temperature of the cooling medium is 20°C. The composition and thermophysical properties of the AISI 304 stainless steel used in the performed simulations are in Tables 3 and 4, respectively:

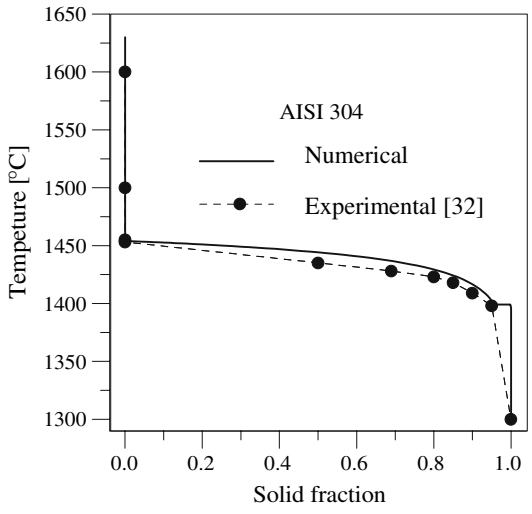


**Fig. 2** Numerical results of the temperature as a function of solid fraction determined by using the Scheil equation [18] and experimental results obtained by Miettinen [32]

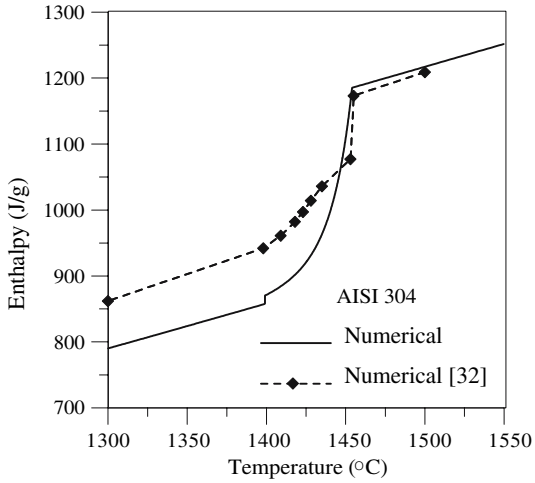


**Fig. 3** Enthalpy variation as a function of temperature, calculated by numerical model and results to the other model in literature [32]

Figure 2 compares numerical results of the solid fraction as a function of temperature determined by using the Scheil equation with experimental results obtained by Miettinen [32]; good agreement is observed.

Figure 3 compares the curve of enthalpy variation versus the temperature, calculated by numerical model with results to the other model in literature [32]. To determine the enthalpy, according to Eqs. 4 and 5, various thermal parameters are needed such as fusion latent heat, thermal conductivity, specific heat, density. The difference between the results obtained in this work and the one presented in the literature [32] can be attributed to the distinct values adopted by these thermal parameters in the simulations. For example,

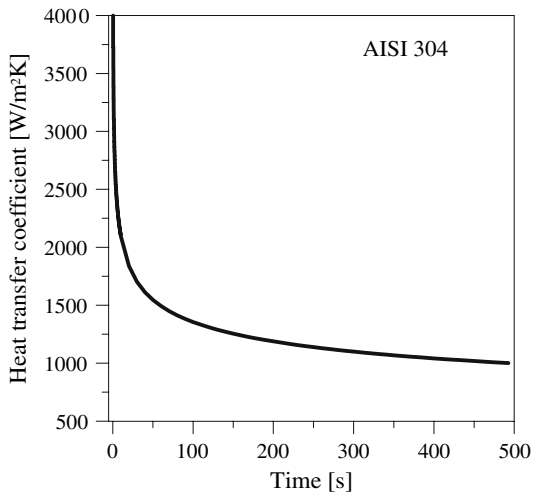


**Fig. 4** Profile of heat transfer coefficient predicted by the numerical model as function of time

the value adopted in this work for the fusion latent heat was 290 (J/g) [31], and the values suggested by Miettinen [32] vary between 180 and 200 (J/g). Analyzing Fig. 2 and 3, one might observe the at the final of the solidification, when the temperature is close to solidus (1399°C), the straight line occurs, that corresponds in Fig. 3 to the vertical lines of constant, for the same temperature.

As for the solidification of casting in a metal mold, the progress of solidification greatly depends upon the heat transfer coefficient at the mold/casting interface and its time dependence. When an air gap at the mold-casting interface is formed during solidification, the heat transfer coefficient will decrease rapidly. The air gap is formed by relative movements of the casting and mold, caused by thermal contraction and expansion

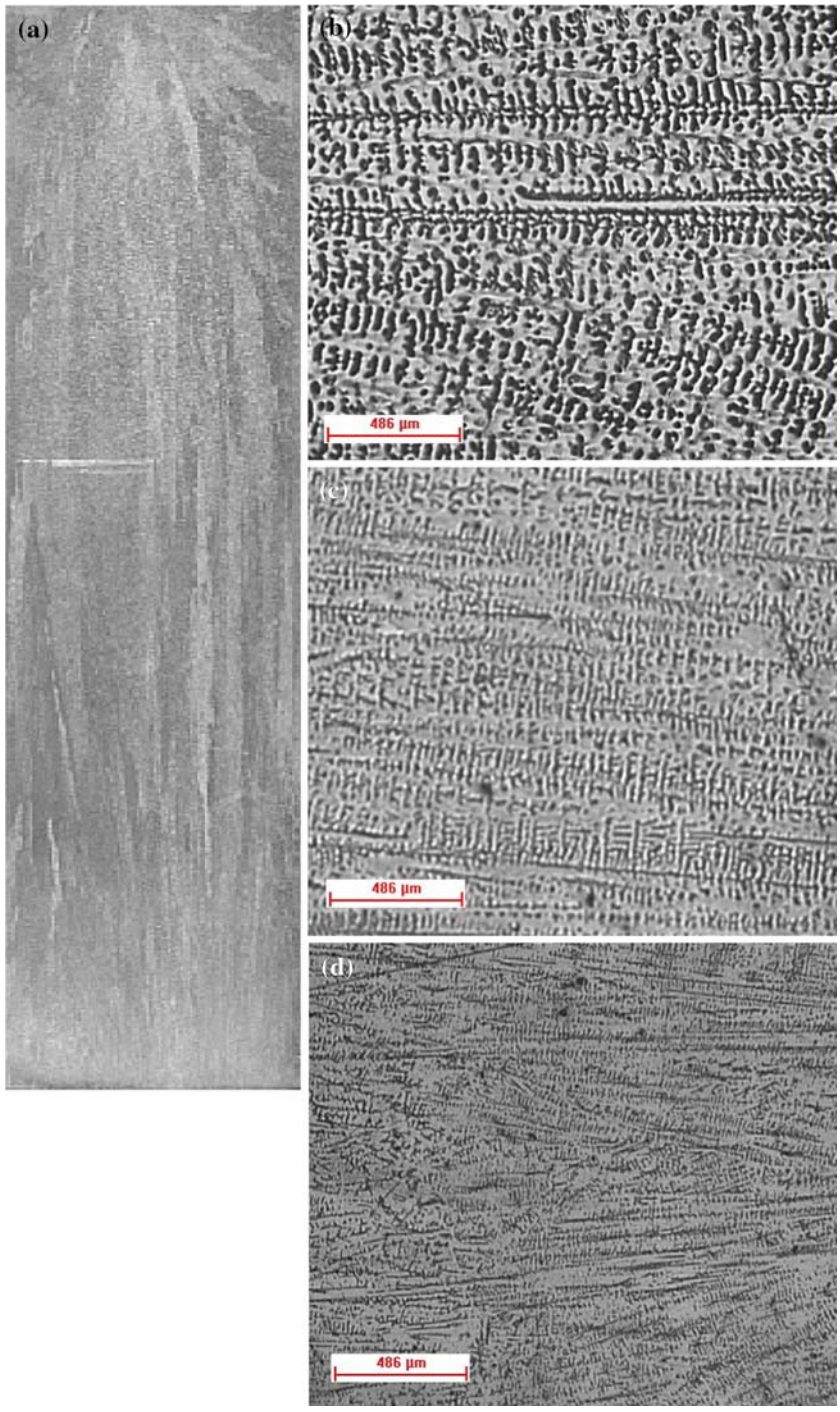


**Fig. 5** Typical solidification structure of a casting directionally solidified AISI 304 stainless steel. (**a**) Macrostructure. Magnification: 1×. Nital attack. (**b**, **c**, **d**) Microstructures of the transverse section showing variation in secondary interdendritic spacings with the distance from the cooled cooper chill (**b**) distance from chill 30 mm, (**c**) distance from chill 10 mm (**d**) distance from chill 1 mm. (**b**, **c**, **d**) Marble attack

during solidification [33]. The heat transfer coefficient is a function of the mold material, the roughness of the mold surface, kinds of coating material and their thickness, etc. If the heat transfer coefficient is extremely small, solidification time will be very long [33, 34].

The variation of heat transfer coefficient at the metal/mold interface was estimated through the adjustment of experimental casting temperature close to the interface and the numerical prediction. The temperature variations experimentally monitored were used in a finite difference heat flow program to determine the transient metal/mold heat transfer coefficient [19]. Figure 4 presents the variation of heat transfer coefficient (*hi*) at metal/mold obtained in this work. The coefficient varies during the solidification process, according to equation:

$$hi(t) = 3250t^{-0.19}\,(\mathrm{W/m^2K}) \tag{15}$$

Figure 5 presents transverse sections microstructures of samples at 30, 10, 1 mm from the metal/mold interface, showing the secondary dendrite arms. It is observed that secondary dendrite arms spacings increase with the distance from the metal/mold interface.

The interdendritic arm spacing variations during solidification were determined using the transient heat transfer coefficient, the temperature variations, the advance velocities of dendrite tip, the local solidification time and the thermal gradients in the front side of the dendrite tip, obtained with the numerical model.

As an example of the numerical model application, Fig. 6 presents the results obtained for cooling rate ($R$)

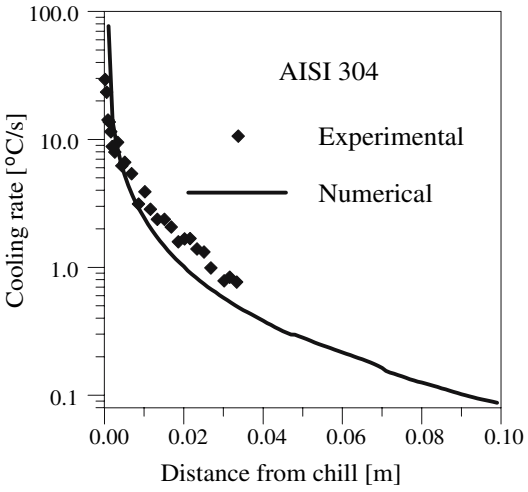


**Fig. 6** Variation of the cooling rate as a function of the distance from chill, numerical and experimental results

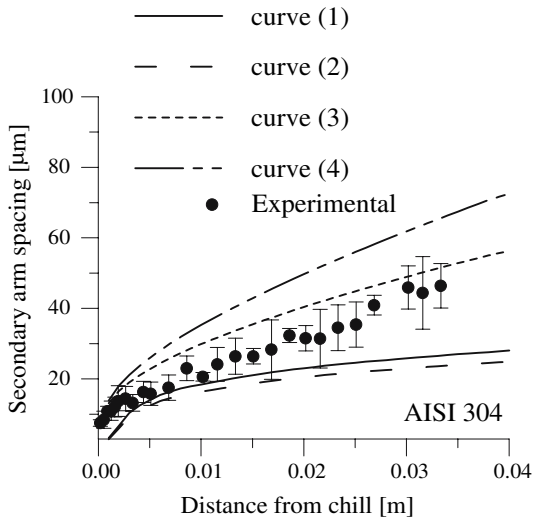


**Fig. 7** Secondary arm spacing curves as function of the distance of the chill, for various equations for several high alloy steels proposed by Taha and collaborators [9] and compared to the experimental results obtained in this work

obtained from equation 15 as function of the distance from chill. It can be seen that the numerical model describes satisfactorily the cooling rate obtained experimentally.

Figure 7 presents the comparison between the experimental results for secondary arm spacing as function of the distance from the metal/mold interface obtained in this work with those obtained by the numerical model using models proposed by different authors [9]. Analyzing Fig. 7, it is observed that the empirical models proposed by Taha and collaborators [9] present the same tendency, however, dislocated with the experimental results; the Eqs. 3 and 4 underestimate the variation of secondary arm spacing and the *curves* 1 and 2 overestimate the variation of secondary arm spacing. The others empirical models proposed for secondary spacing [2, 30] were also tested but the results obtained did not describe satisfactorily the experimental observation. It must be emphasized that the models are not necessarily incorrect but inadequate for the solidification conditions observed in this work.

The secondary arm spacings obtained in this work were measured as function of the distance from the metal/mold interface. According to Taha and collaborators, no systematic influence of the gradient exists, but as expected, the spacings decrease with increasing cooling rate because the local solidification time during which the material was in the heterogeneous state and in the coarsening occurred, decreases with cooling rate.

So, from secondary spacing experimental measures ($\lambda_2$) as function of the chill distance and from the

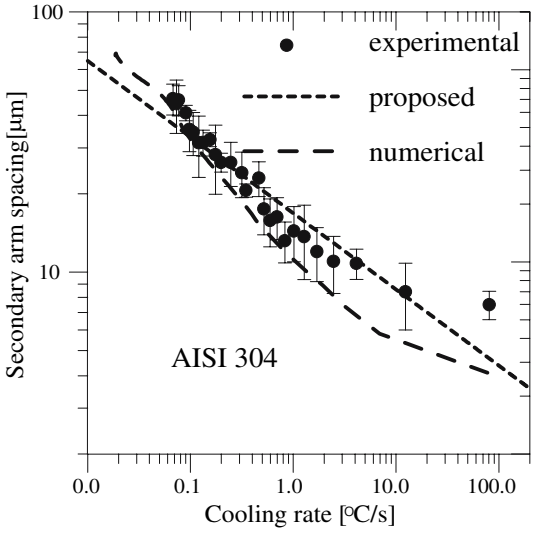


**Fig. 8** Numerical and experimental correlation between the secondary spacing as the function the cooling rate of the AISI 304 stainless steel solidified unidirectionally

cooling rate measures ($R$) for different positions, the following correlation was obtained:

$$\lambda_2 = 16.8R^{-0.29}\,(\mu\text{m}) \tag{16}$$

Where the spacings are in μm and the cooling rate in °C/s.

Figure 8 presents the comparison between the experimental results for secondary arm spacing as the cooling rate function obtained in this work with those obtained by the numerical model using the proposed equation. It suggests that the proposed equation describes well the variation of secondary arm spacing found in the present work, but that one for cooling rate below 1°C/s underestimates the variation of secondary arm spacing.

## Conclusions

Numerical and experimental results presented in this paper indicate that the numerical model permits a precise analysis of the AISI 304 stainless steel microstructure formation. This model determine temperature profiles, heat transfer coefficient, thermal parameters (thermal gradients, tip rate movement, rate cooling, local solidification time), and finally, microstructural parameters (interdendritic spacing).

For accomplished experimental conditions, the results for the heat transfer coefficient in function of time for AISI 304 stainless steel are:

$$hi(t) = 3250t^{-0.19}\,[\text{W/m}^2\text{K}] \tag{15}$$

For the case of the experimental apparatus used (vertical directional solidification) and for the AISI 304 stainless steels a columnar structure was formed in big extension of the samples. The secondary arm spacings were measured along the distance from the chill as function of the distance from the metal/mold interface and it was observed that the secondary arm spacings decreases with cooling rate, according to the equation:

$$\lambda_2 = 16.8R^{-0.29}\,(\mu\text{m}) \tag{16}$$

Thus, it is possible to conclude that for high heat transfer coefficient, local solidification time is reduced, and, as a consequence, secondary spacing is small (refined structure) with better mechanical properties. On the other hand, a low heat transfer coefficient increases the local solidification time; therefore, secondary spacing is large (coarse structure). This is very important because the relation of the mechanical properties (strength, ductility and fatigue life) is the insight for the design of structural castings. The improved properties of fine-grain-sized casting are due to finer distribution of microporosity and second-phase particles.

The utility of applying the model to the solidification of castings with transient conditions of heat extraction is to analyze the influences in the microstructure formation and for future predictions of dendrite arm spacings variations.

**Acknowledgements** The authors would like to acknowledge financial support provided by FAPESP (The Scientific Research Foundation of the State of São Paulo, Brazil) Proc. 02/02060-6.

## References

1. Inoue Y, Kikuchi M (2003) Nippon Steel Technical Report 88:62
2. Brooks JA, Baskes MI, Greulich FA (1991) Metall Trans A 22:915
3. Vitek JM, Dasgupta A, David SA (1983) Metall Trans A 14:1833
4. Suutala N, Takalo T, Moisio T (1979) Metall Trans A 10:512
5. Callister WD Jr (1993) Materials science and engineering—an introduction. John Wiley & Sons, NY
6. Kawaguchi Y, Shirai Y (2002) J Nucl Sci Technol 39:1033
7. Rao KBS, Valsan M, Srinivasan VS, Mannan SL (1994) J Eng Mater Technol 116:193
8. Kurz W, Fisher DJ (1992) Fundamentals of solidification. Trans Tech Publications, Aedermannsdorf
9. Taha MA, Jacobi H, Imagumbai M, Schwerdtfeger K (1982) Metall Trans A 13:2131
10. Piwonka TS, Flemings MC (1966) Trans TMS-AIME 236:1157
11. Poirier DR, Yeum K, Maples AL (1987) Metall Trans A 18:1979

12. Kubo K, Pehlke RD (1985) Metall Trans B 16:359
13. Argo D, Gruzleski JE (1989) AFS Trans 96:67
14. Melo MLNM, Rizzo EMS, Santos RG (1997) Mater Sci Forum 242:83
15. Pequet Ch, Gremaud M, Rappaz M (2002) Metall Trans A 33:2095
16. Melo MLNM, Rizzo EMS, Santos RG (2005) J Mater Sci 40:1
17. Rappaz M, Stefanescu DM (1988) Metals handbook, vol 15. ASM, Ohio, USA, p 883
18. Batthe TP, Pehlke RD (1989) Metall Trans B 20:149
19. Melo MLNM, Rizzo EMS, Santos RG (2004) Mater Sci Eng A 374:351
20. Pan EN, Lin CS, Loper CR Jr (1990) AFS Trans 98:735
21. Suri VK, Paul AJ, Berry JT (1994) AFS Trans 102:861
22. Laurent V, Rigaut VC (1992) AFS Trans 100:647
23. Flemings MC (1974) Solidification processing. McGraw-Hill, New York, p 234
24. Young KP, Kirkwood DH (1975) Metall Trans A 6:197
25. Huang H, Berry JT (1993) AFS Trans 101:669
26. Bower TF, Brody HD, Flemings MC (1966) Trans AIME 236:624
27. Hunt JD, Lu SZ (1996) Metall Trans A 27:611
28. Trivedi R (1984) Metall Trans A 15:977
29. Feurer U (1977) Proceedings of the symposium on quality control of engineering alloys, Delft, p 131
30. Pryds NH, Huang X (2000) Metall Mater Trans A 31:3155
31. Pehlke RD, Jayarajan A, Wada H (1992) Summary of thermal properties for casting alloys and mold materials. University of Michigan, Ann Arbor, MTIS-PB83-211003
32. Miettinen J (1994) Metall Trans B 28:909
33. Griffiths WD (2000) Metall Mater Trans B 31:285
34. Nishida Y (1987) Metall Mater Trans B 17:281